Geochemistry Geophysics Geosystems G3

Article
Volume 15, Number 2
28 February 2014
doi: 10.1002/2013GC004940
ISSN: 1525-2027

Published by AGU and the Geochemical Society

The late Pliocene Benguela upwelling status revisited by means of multiple temperature proxies

Guillaume Leduc
Institute of Geosciences, University of Kiel, Kiel, Germany

Now at CEREGE, UMR7330, Aix-Marseille Université, CNRS, IRD, Europôle de l'Arbois, BP80, 13545, Aix-en-Provence CEDEX 4, France (leduc@cerege.fr)

Dieter Garbe-Schönberg and Marcus Regenberg
Institute of Geosciences, University of Kiel, Kiel, Germany

Camille Contoux
Laboratoire des Sciences du Climat et de l'Environnement/IPSL, CEA-CNRS-UVSQ, UMR8212, Orme des Merisiers, CE Saclay, Paris, France

SISYPHE, Université Pierre et Marie Curie & CNRS, UMR7619, Paris, France

Johan Etourneau
LOCEAN, CNRS/UPMC/IRD/MNHN, UMR7159, Paris, France

Ralph Schneider
Institute of Geosciences, University of Kiel, Kiel, Germany

[1] As compared to the late Pleistocene, Alkenone-based sea surface temperature (SST) in the Benguela region revealed relatively warm and stable SST recorded between ~3.5 and 2.0 Ma, and coincide with a period of increasing biological productivity as revealed by increasing deposition of biogenic opal. We assess how the hydrological patterns recorded in SST proxies are embedded in the geological record by performing a proxy-proxy comparison. We used Laser-Ablation Inductively Coupled Plasma-Mass Spectrometry to measure the Mg/Ca on the planktonic foraminifera species *Globigerina bulloides*, allowing in situ measurements of Mg/Ca on individual foraminiferal tests. Mg/Ca-derived temperatures provide much colder temperatures than alkenone-derived SST by up to 10°C. We build a scenario involving contrasting sensitivities of paleothermometers upon the annual cycle, namely alkenones preferentially capturing SST when the surface ocean is warmer than the mean-annual average SST, and *G. bulloides* capturing SST when upwelling intensifies. Multichamber analysis also suggests that *G. bulloides* migrates below the sea surface while calcifying its last chambers prior to gametogenesis, allowing the extraction of both surface and subsurface temperature from Mg/Ca measured on different chambers. The range of temperatures recorded between our multiple SST proxies is supported by the range of temperatures simulated with a general circulation model when different seasons, different water depth and different orbital configurations occurring during the late Pliocene are considered. A greater seasonal cycle in SST during the Pliocene can account for alkenone and Mg/Ca-derived temperature contrast, pointing to a radically different mode of upwelling activity in the Benguela region compared to today.

Components: 10,386 words, 7 figures, 1 table.

Keywords: late Pliocene; sea surface temperatures; Mg/Ca.

Index Terms: 4964 Upwelling: Paleoceanography; 4279 Upwelling and convergences: Oceanography: General; 4954 Sea surface temperature: Paleoceanography; 4926 Glacial: Paleoceanography; 4928 Global climate models: Paleoceanography; 1626 Global climate models: Global Change; 3337 Global climate models: Atmospheric Processes.

Received 11 July 2013; **Revised** 20 November 2013; **Accepted** 2 December 2013; **Published** 28 February 2014.

Leduc, G., D. Garbe-Schönberg, M. Regenberg, C. Contoux, J. Etourneau, and R. Schneider (2014), The late Pliocene Benguela upwelling status revisited by means of multiple temperature proxies, *Geochem. Geophys. Geosyst.*, *15*, 475–491, doi:10.1002/2013GC004940.

1. Introduction

[2] The late Pliocene (~3.3–3 Ma) was marked by warmer and more stable climatic conditions than the late Pleistocene (see e.g., *Dowsett et al*. [2009] for the late Pliocene ocean status), and is often used to understand climate behavior for a globally warmer planet. As such, this time period has been the focus of many paleoclimate modeling studies in the frame of the Pliocene Model Intercomparison Project (PlioMIP, see *Haywood et al*. [2013a] for a synthesis of the results). Sea Surface Temperature (SST) reconstructions are in turn used as benchmarks to evaluate the performance of climate models for simulating the late Pliocene climate, and model/data comparison ultimately helps identifying model deficiencies in simulating some aspects of regional climate conditions over periods of sustained global warmth [*Dowsett et al*., 2012]. Identified model deficiencies might ultimately serve as guidance for improving climate models involved in future climate projections [*Braconnot et al*., 2012].

[3] Even though the model/data comparison of Pliocene SST was generally found to be satisfactory, some pervasive regional model-data mismatches were spotted [*Dowsett et al*., 2012]. Among other places, significant model/data SST mismatches were identified in eastern boundary upwelling regions such as the Benguela Upwelling System (BUS, Figure 1) [*Dowsett et al*., 2012]. Alkenone-based SST has previously been reported to vary between ~27 and 24°C during the late Pliocene in the BUS, along with a series of short-lived periods when SST dropped below 22°C that occurred during the early Pleistocene (Figure 2) [*Etourneau et al*., 2009; *Rosell-Melé et al*., 2014]. In the meantime, a transient increase in opal accumulation rates has been recorded between ~3.5 and 2.2 Ma, probably reflecting an intensification of seasonally pulsed diatom productivity associated with a strengthening of the BUS activity and/or with intensified silicate supply to the thermocline [*Lange et al*., 1999; *Berger et al*., 2002; *Etourneau et al*., 2012] (Figure 2). Such patterns cannot be easily reconciled with the general view that increased

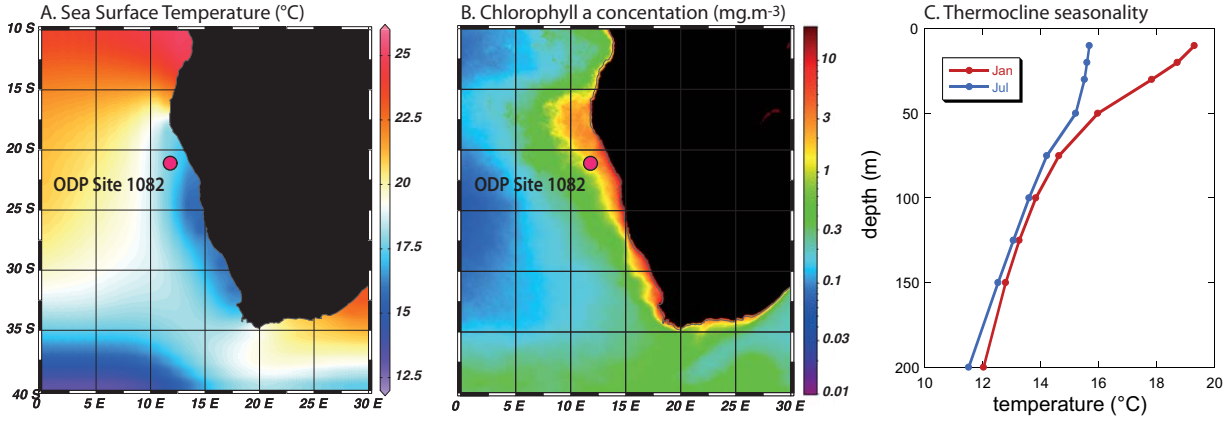

Figure 1. (a) Annual-mean SST in the southeastern Atlantic Ocean extracted from the World Ocean Atlas 2005 [*Locarnini et al*., 2006]. (b) Annual-mean *Chlorophyll a* concentration derived from SeaWIFS imaging (http://seawifs.gsfc.nasa.gov/). (c) Seasonal temperature profile across the upper 200 m water depth at ODP 1082 site extracted for January and July from the World Ocean Atlas 2005 [*Locarnini et al*., 2006]. Red dot in Figures 1a and 1b indicates ODP 1082 site location.

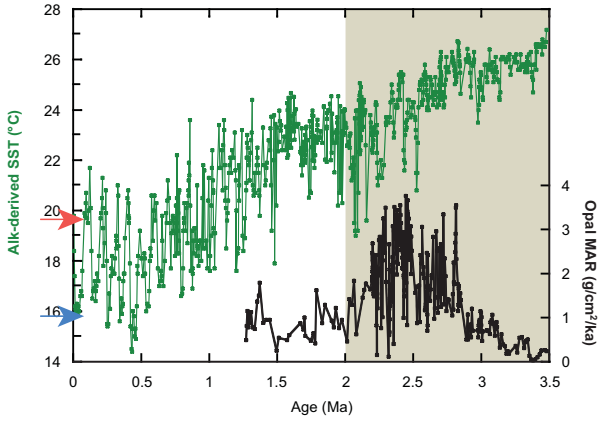

Figure 2. Alkenone-derived SST evolution over the last 3.5 Ma (green curve) and biogenic opal mass accumulation rates (MAR, black curve) at ODP site 1082 [*Etourneau et al*., 2009]. The gray box highlights the late Pliocene time interval of interest, when an increase in opal MAR was associated with only moderate SST drop. Red and blue arrows on the *y* axis indicate present-day SST for January and July, respectively.

upwelling activity might co-occur with decreased SST as observed in the modern ocean. If strong upwelling activity prevailed when diatom productivity was highest, co-occurring warm and stable temperatures might either indicate that alkenone-derived SST primarily captures the nonupwelling season, or that nutrient-rich waters upwelled at studied site were much warmer than today [*Dekens et al*., 2007].

[4] In the modern BUS, Ekman transport advects surface waters offshore that are subsequently replaced by cold, nutrient-rich subsurface waters associated with the shoaling of the regional thermocline (Figure 1). Whether climate models simulating the late Pliocene can capture subtle changes in the thermocline structure in dynamic environments such as upwelling systems is a source of concern, because general circulation models (GCMs) have a coarse resolution, the width of upwelling systems (∼250 km) being comparable to the size of a typical GCM grid. There is, however, growing evidence that marine paleothermometers can be skewed toward specific seasons, making SST estimations reflective of periods warmer or colder than the mean-annual SST depending upon the proxy used [*Leduc et al*., 2010a; *Schneider et al*., 2010; *Lohmann et al*., 2013; *Wang et al*., 2013]. Consequently, in highly dynamical regions such as in upwelling systems, the estimated SST from planktonic organisms might depend on the ecological niches that they occupy. Prior to any attempt to evaluate climate model performance in these regions, it is hence crucial to better characterize how SST signals are captured by planktonic organisms and transmitted to the geological archives.

[5] We here reassess the late Pliocene SST status within the BUS by performing a proxy-proxy comparison. We measured Mg/Ca on the planktonic foraminifer *Globigerina bulloides* in the BUS, one species notoriously known to proliferate where and when high primary productivity prevails [*Giraudeau*, 1993; *Žarić et al*., 2005; *Lombard et al*., 2011]. In addition, *G. bulloides* is known to migrate from the surface to the upper thermocline prior to gametogenesis [*Schiebel and Hemleben*, 2005; *Erez et al*., 2003; *Marr et al*., 2011], so that Mg/Ca measurements performed on different foraminiferal chambers that calcified at different water depths would provide a highly spatially resolved analysis of migratory species. We explore such possibility by using Laser Ablation-Inductively Coupled Plasma-Mass Spectrometry (LA-ICP-MS) to measure Mg/Ca on different chambers from individual foraminifera analysis. These measurements help reconstructing seasonal and vertical temperature gradients and inferring the upper ocean temperature variability within the BUS during the Late Pliocene epoch.

2. Regional Settings

[6] The BUS extends from the southern South African to the northern Namibian coasts (Figure 1). Among the four eastern boundary upwelling systems, the BUS is nowadays the upwelling region where primary productivity is highest and seasonality is lowest, with relatively cold surface waters and high primary productivity occurring year-round (Figure 1) [*Chavez and Messié*, 2009]. ODP site 1082 (21°06′S, 11°49′E, 1279 m water depth) is situated at the northwestern edge of the northern BUS, where SST seasonality reaches ∼4°C (Figure 1c). Surface currents flow along the South Africa, Namibia and Angola shorelines, above which upwelling-favorable winds prevail [*Chavez and Messié*, 2009]. ODP site 1082 lies within the Benguela Coastal Current (BCC), which represents the northward-flowing branch of the broader Benguela Current (BC) [*Moroshkin et al*., 1970]. The annual cycle of SST is 4–5°C in magnitude, ranging from ∼15 to 20°C between austral winter and summer, respectively [*Locarnini et al*., 2006] (Figure 1). At ∼15°S, the BCC meets the warm and nutrient-depleted waters of the southward-flowing Angola

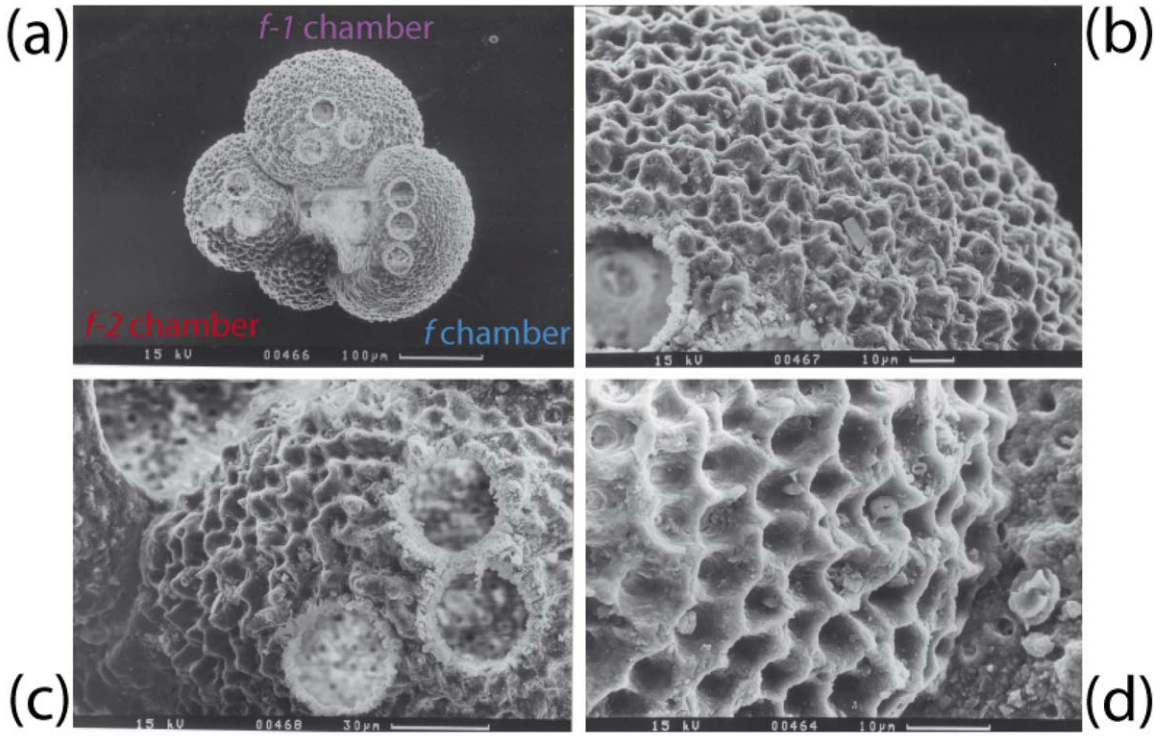

Figure 3. SEM micrographs of *G. bulloides*. (a) Whole *G. bulloides* specimen dated at 2.19 Ma showing the three laser ablation pits on the final *f*, penultimate *f-1*, and antepenultimate *f-2* chambers. (b–d) Detailed wall textures of *G. bulloides* tests for foraminifera dated at 2.23, 2.74, and 3.37, i.e., for times when high, intermediate and low opal MAR were recorded, respectively.

Current, where much larger SST seasonality than at ODP 1082 site is thought to impact both modern-day and late Pleistocene surface waters [*Hessler et al*., 2011]. Occasionally, mesoscale tongue-like southward intrusions of the Angola current reaching ODP 1082 site can lead to extreme subseasonal SST variability during austral summer [*Shannon et al*., 1985].

[7] The upwelling season occurs mainly during the austral winter when winds intensify, but the thermocline depth remains relatively shallow year-round (Figure 1). The modern annual cycle of SST and primary productivity within the BUS is, however, less marked than in other eastern boundary upwelling systems because eddies induce high-frequency intraseasonal hydrological variations [*Chavez and Messié*, 2009].

3. Theoretical Background on SST Proxies Specificities

[8] Alkenone-derived SSTs estimated from core-top sediments from the Southeastern Atlantic Ocean capture well the mean-annual SST from very different biogeochemical provinces [*Müller et al*., 1998]. One sample collected very close to ODP site 1082, however, indicates alkenone-based SST significantly warmer than the mean-annual modern SST (see *Müller et al*., 1998, Figure 3). Recently, a compilation of sediment trap time series revealed that seasonality in alkenone fluxes to the seafloor vary largely across the oceans, but without any distinguishable pattern that can consistently explain the data set as a whole [*Rosell-Melé and Prahl*, 2013]. Regardless whether alkenone-based temperatures might be attributed to the mean-annual SST or might be seasonally skewed in the southeastern Atlantic ocean, an alkenone-derived SST drop recorded over the last decades associated with a recent upwelling-induced cooling trend within the BUS demonstrates the ability of alkenones to capture recent SST changes [*Leduc et al*., 2010b; *Narayan et al*., 2010].

[9] At ODP site 1082, core-top planktonic foraminifera assemblages are dominated by the subpolar species *G. bulloides* and *Neogloboquadrina pachyderma* (right coiling) [*Giraudeau*, 1993]. High abundance of *G. bulloides* at low latitudes is globally associated with upwelling environments

[*Lombard et al*., 2011], one ecological characteristic used to reconstruct primary productivity of tropical upwelling systems by means of *G. bulloides* countings [*Gupta et al*., 2003; *Bassinot et al*., 2011]. We hence anticipate the Mg/Ca-derived SST reconstruction based on that species to be reflective of seasons with SST below the mean-annual SST, i.e., when upwelling intensifies.

[10] Apart from the affinity of *G. bulloides* with environments where high primary productivity prevails, the *G. bulloides* life cycle is worth being considered while attempting to reconstruct the upper water column structure. Adult specimens of *G. bulloides* dwell in shallow waters and reproduce once per month, following lunar cycles [*Schiebel and Hemleben*, 2005]. Prior to gametogenesis—which immediately precedes the death of the foraminifer—*G. bulloides* migrates downward within the thermocline [*Schiebel and Hemleben*, 2005] where it calcifies its last chambers, so these last chambers should sample subsurface waters instead of surface waters. Additional evidence for such impact of *G. bulloides* ontogeny comes from recent studies based on Mg/Ca measurements performed on multiple chambers [*Marr et al*., 2011], as well as a relationship between *G. bulloides* test size and *G. bulloides* Mg/Ca [*Friedrich et al*., 2012] and $\delta^{18}O$ [*Birch et al*., 2013]. We will use jointly the *G. bulloides* ontogeny and ecological niche to track temperature changes across a range of different depths over periods of intensified upwelling by measuring Mg/Ca on different *G. bulloides* chambers.

4. Methods

[11] The ODP site 1082 age model is extensively described in *Etourneau et al*. [2009], and is based on the comparison of the alkenone-based SST record with the benthic stack of *Lisiecki and Raymo* [2005]. In our study, *G. bulloides* were picked from the >255 μg size fraction. Even though the sedimentary sequence was retrieved well above the water depth where calcite dissolution is supposed to take place in the tropical Atlantic Ocean [*Regenberg et al*., 2006], Pliocene-age foraminiferal preservation was monitored through Scanning Electron Miscroscopy (SEM) to ensure that no bias associated with calcite dissolution have impacted Mg/Ca-based SST estimation [*Regenberg et al*., 2006; *Tachikawa et al*., 2008]. SEM pictures revealed well-preserved foraminiferal tests with apparent patterns of interpore ridges (Figure 3), synonym of a good preservation as reported in an ultrastructure study of *G. bulloides* tests from the South Atlantic Ocean [*Dittert and Henrich*, 2000].

[12] Foraminifera were mounted with adhesive pads onto glass slides and arranged within a large volume ablation cell (Zurich LDHCLAC ablation cell, [*Fricker et al*., 2011]) without any cleaning procedure. We obtained laser ablation depth profiles using an ArF excimer laser operating at 193nm (GeoLasPro Plus, Coherent/Lambda Physik, Germany). The spot size was 30 μm in diameter. Energy density at the sample surface was kept at 2 mJ/cm^2, with a pulse frequency of 10 Hz. The ablated material was carried to the ICPMS (Agilent 7500s with a Ni interface) using 1 L/min He as the carrier gas that was mixed with 0.8 L/min Ar prior to injection into the ICP. The integration time was 20 ms per m/z in transient mode. We used ^{44}Ca as an internal standard for quantification and NIST612 [*Jochum et al*., 2011] for calibration and data integration with GLITTER software (see below). A pressed powder tablet of ECRM-752 [*Greaves et al*., 2008] was analyzed with each sample batch at the beginning and end of each session as an unknown sample. Element concentrations were measured using ^{24}Mg, ^{27}Al, ^{44}Ca, ^{55}Mn, ^{85}Rb, ^{88}Sr, with typical relative standard deviations of the element/Ca ratios lower than 5% based on repeated analysis of NIST612 (n = 27).

[13] We performed repeat Mg/Ca analysis from the same sedimentary horizons to provide snapshots of past changes in water column dynamics and, by extension, in the amplitude and frequency of upwelling events. We have analyzed ~1300 profiles from 16 sediment horizons dated between ~3.5 and 2.0 Ma, i.e., encompassing the increased biogenic opal Mass Accumulation Rate (MAR, Figure 2). Between 4 and 15 foraminiferal tests were analyzed for each horizon. Those measurements were performed on the final (f), penultimate (f-1), and antepenultimate (f-2) chambers, and repeated three times for each chamber to allow comparison of intrachamber, interchamber, and interspecimen Mg/Ca heterogeneity (Figure 3 and Table 1).

[14] We first screened the obtained LA-ICP-MS profiles in order to remove those sections that appeared to show contamination of the tests by clays and/or authigenic contaminants, which usually affect the inner and outer parts of the test. The integration window was set manually using the

Table 1. Data Used to Compute Figure 5 (Error Bars From Figure 5 are Interforam RSD)[a]

					f chamber				*f-1 chamber*				*f-2 chamber*			
Sample	Depth (mbsf)	Depth (mcd)	Age (ka)	#forams	Intrachamber SST RSD (°C)	Interforam mean Mg/Ca (mmol/mol)	Interforam mean SST (°C)	Interforam SST RSD (°C)	Intrachamber SST RSD (°C)	Interforam mean Mg/Ca (mmol/mol)	Interforam mean SST (°C)	Interforam SST RSD (°C)	Intrachamber SST RSD (°C)	Interforam mean Mg/Ca (mmol/mol)	Interforam mean SST (°C)	Interforam SST RSD (°C)
1082A-24X-2-17cm	217.18	232.84	2229	13	3.48	1.85	12.69	2.63	2.82	2.24	14.59	1.72	5.74	2.33	14.99	2.22
1082A-24X-3-62cm	218.88	234.54	2236	9	5.36	2.45	15.51	4.26	4.76	3.16	18.04	2.19	3.08	3.79	19.87	2.58
1082A-27X-1-12cm	244.52	260.18	2429	7	5.96	1.59	11.19	1.09	5.09	2.03	13.63	2.36	6.47	2.47	15.57	1.74
1082A-27X-1-115cm	245.55	261.21	2435	14	5.21	2.17	14.27	3.05	3.90	2.74	16.60	3.57	3.02	3.10	17.84	4.13
1082A-28X-2-62cm	256.12	271.78	2525	12	2.92	2.18	14.35	3.45	3.52	2.58	16.02	3.46	3.13	2.83	16.93	3.38
1082A-29X-2-115cm	266.25	281.91	2587	7	2.90	2.71	16.50	2.66	1.75	3.54	19.19	1.84	1.84	3.72	19.69	1.64
1082A-30X-2-62cm	275.42	291.08	2645	4	3.24	2.17	14.31	1.80	1.94	2.37	15.17	2.41	4.96	2.23	14.55	3.96
1082A-32X-4-12cm	297.12	312.78	2743	15	5.19	2.50	15.71	2.43	8.24	3.16	18.03	2.61	7.53	3.39	18.74	2.29
1082A-34X-1-12cm	311.82	327.48	2825	10	3.36	2.17	14.28	1.61	3.63	3.02	17.61	1.93	3.74	3.82	19.94	1.47
1082A-35X-1-112cm	322.52	338.18	2898	10	3.70	2.49	15.67	2.68	3.14	3.11	17.90	3.82	2.59	3.54	19.19	3.15
1082A-35X-3-12cm	324.52	340.18	2908	7	4.01	2.41	15.34	1.62	2.85	2.75	16.66	1.57	3.13	2.96	17.40	n.d.
1082A-38X-6-49cm	348.59	364.25	3117	9	3.36	2.08	13.87	2.59	4.51	2.12	14.06	3.50	5.49	2.16	14.25	3.06
1082A-39X-1-119cm	351.49	367.15	3135	11	2.72	2.18	14.34	1.54	4.06	2.97	17.43	2.65	2.79	3.46	18.96	2.77
1082A-41X-3-21cm	372.71	388.37	3367	6	3.34	2.10	13.94	2.77	3.82	2.62	16.18	2.71	3.77	3.05	17.68	2.72
1082A-42X-1-19cm	379.39	395.05	3465	9	2.43	2.19	14.38	2.76	2.44	2.98	17.48	1.59	3.60	3.40	18.77	2.60
1082A-42X-1-80cm	380	395.66	3472	10	2.75	2.94	17.33	2.86	5.29	3.01	17.56	2.52	5.79	3.34	18.61	2.91

[a]Also reported are means intrachamber RSD to visualize reproducibility of SST estimates based on LA profiles.

GLITTER software package (Macquarie University), and all the profiles were integrated using only signal intensities but neglecting software output for Mg and Ca concentrations. This procedure ensures the integrity and reproducibility of the integration method. The time window of the test ablation was deduced through visual inspection of the shape of the Ca and Sr intensity profiles using the GLITTER software (Figure 4). Other elements were used to monitor contaminant phases, in order to ensure proper integration of Mg/Ca by avoiding those parts of the test where Mg is unrelated to biomineralized calcite. Rubidium (Rb) and Al, which are associated with clays adhering to the inner and outer parts of the tests, were used to remove parts of the integration windows where spikes in Mg are associated with spikes of Rb and Al (Figure 4). Strontium (Sr) was used to identify parts of the test affected by severe alteration, which has never been the case within our samples. Anomalously high Mn is usually associated with Mg-rich contaminant phases consisting of authigenic Mn-rich carbonates and ferromanganese oxides [*Pena et al*., 2008]. Important increases in Mn intensity were removed from the laser ablation profiles to avoid any bias in Mg/Ca toward anomalously high values (Figure 4) [*Pena et al*., 2005, 2008]. In general, the LA profiles and element/Ca values obtained are similar to the ones obtained from core tops published in *Marr et al*. [2011], suggesting that diagenetic recrystallization does not alter Mg/Ca.

[15] Once the profiles were integrated with the GLITTER software, a second screening of the full data set was performed to ensure removing inconsistent concentrations that were not detected on the basis of simple visual inspection of the elemental profiles. For this second screening step, the intrachamber relative standard deviation (RSD) was computed using the triplicate analyses performed on each chamber, and was used as an independent estimate of the efficiency of the first data screening step that was using the GLITTER software. In most cases, the intrachamber RSD of Mg/Ca was better than 5%, i.e., comparable to the RSD estimated from standard analysis. When the RSD was larger than 10%, anomalous Mg/Ca values of LA profiles were systematically screened for possible alteration and/or contamination by checking other element/Ca ratios. RSD larger than 10% occurred in about 5% of the analyzed chambers; about half of those anomalously high intrachamber RSD were due to one of the LA profiles for which some element/Ca values unambiguously

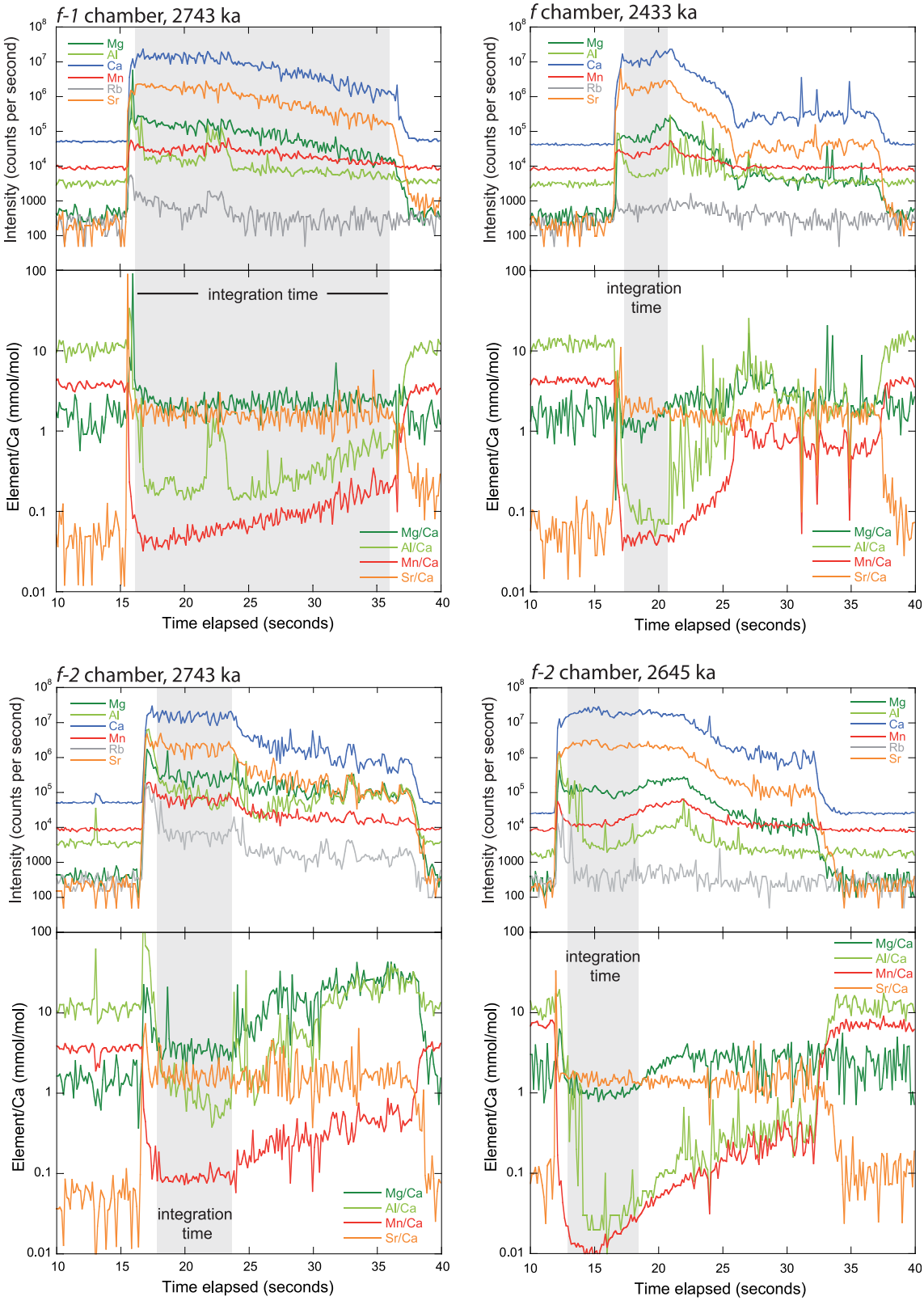

Figure 4. Typical LA profiles used to screen geochemical data for contaminated sections of the tests chambers. (top) Raw elemental intensities and (bottom) element/Ca ratios. Gray vertical band indicates the integration time over which the element/Ca ratios were computed.

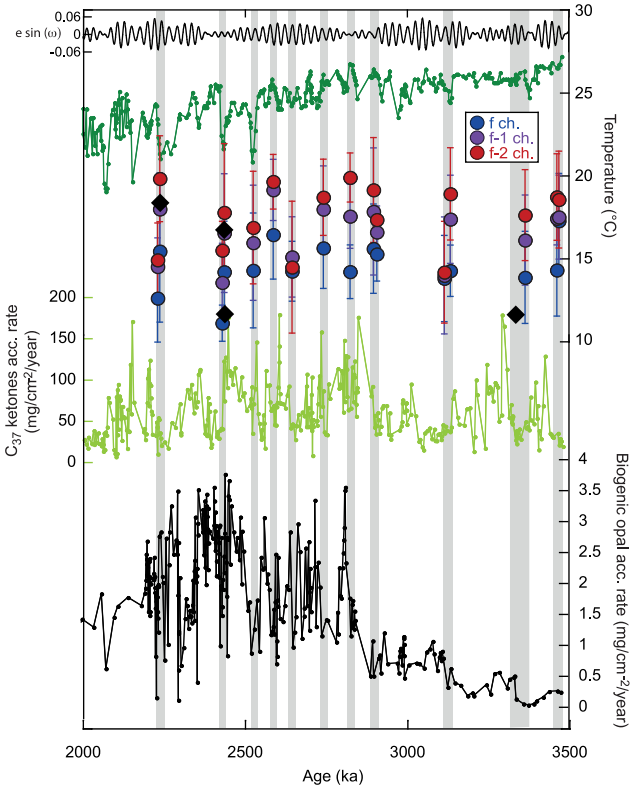

Figure 5. Late Pliocene multiproxy records of temperature and productivity. Temperature estimated from alkenones (dark green), from Mg/Ca measured by LA-ICP-MS on different chambers from multiple specimens (blue, purple, and red colors) and by ICP-OES on multiple *G. bulloides* specimens (black diamonds) are converted to temperature on the same *y* axis (error bars denote interforam temperature RSD for each chamber). Also shown are total C_{37} alkenones MAR (light green) and opal MAR (black curve). Temporal changes in the precessional parameter are reported on top of the figure (sinusoid black curve) [*Laskar*, 1990]. Vertical gray bars indicate time intervals where abundant *G. bulloides* were found, and subsequently targeted for Mg/Ca measurements. The standard errors associated with temperature estimates are ~1°C for both alkenones and Mg/Ca [*Rosell-Melé et al*., 2001; *Greaves et al*., 2008].

pointed to contamination by clays or Mn hydroxides not apparent within the first screening step. Those anomalous LA profiles, once discarded, lead to intrachamber RSD of Mg/Ca values lower than 5%, ensuring the integrity of the data set as a whole.

[16] For some horizons where *G. bulloides* specimens were abundant enough, we also measured Mg/Ca in bulk samples. Approximately 10 tests of *G. bulloides* were measured for Mg/Ca. Tests were gently crushed and cleaned following the standard procedure including a reductive step as detailed in *Martin and Lea* [2002]. Samples were analyzed by Inductively Coupled Plasma-Optical Emission Spectrometry (Spectro Ciros SOP) with cooled cyclonic spraychamber and microconcentric nebulization (200 μL min^{-1}). Intensity ratio calibration followed the method of *de Villiers et al*. [2002]. Instrumental error was ±0.3% RSD, as indicated by replicate standards. All Mg/Ca measurements presented in this study were performed at Kiel University.

[17] *G. bulloides* is a nonsymbiotic species that does not form gametogenic calcite [*Spero and Lea*, 1996]. We hence neglect potential Mg/Ca artifacts associated with vital effects and/or gametogenic processes that may modify the incorporation of Mg into the calcite test in some planktonic foraminifera species other than *G. bulloides* [*Sadekov et al*., 2005]. To interpret interchamber and intertest Mg/Ca variability, we will rely only on *G. bulloides* ecology.

[18] To translate the *G. bulloides* Mg/Ca into temperature, several approaches have been applied. Calibration equations for *G. bulloides* were developed using sediment trap, core top, and culturing data [*Lea et al*., 1999; *Elderfield and Ganssen*, 2000; *McConnell and Thunell*, 2005; *Cléroux et al*., 2008; *Marr et al*., 2011], each approach having advantages and disadvantages [*Barker et al*., 2005]. Because we are interested in environmental parameters such as seasonality and water depth when/where *G. bulloides* thrives, we use the calibration based on calcification temperature of *Elderfield and Ganssen* [2000], while recognizing that large uncertainties on *G. bulloides* δ^{18}O might obscure such a calibration method [*Elderfield and Ganssen*, 2000; *Mortyn and Charles*, 2003; *Skinner and Elderfield*, 2005]. We, however, note that this calibration agrees well with the one derived from the culturing study of *Lea et al*. [1999].

[19] One way to test the validity of our conceptual model is to compare alkenone and Mg/Ca reconstructed temperatures with Pliocene climate model outputs. As our foraminifera sampling is highly irregular and the age model cannot unambiguously determine under what orbital configuration temperature signals have been fossilized, our results must be compared to model simulations using different orbital configurations. This provides a way to encompass a wider range of climatic backgrounds that likely occurred over the late Pliocene time window. We thus compare our results to mid-Pliocene model simulations using the IPSL-CM5A atmosphere ocean general circulation model (AOGCM) [*Contoux et al*., 2012]. Atmospheric

resolution is 3.75° in longitude by 1.9° in latitude, with 39 vertical levels. Oceanic resolution is ∼2° in the Benguela current region, with 31 vertical levels. Boundary conditions such as topography, reduced ice-sheet extent, and vegetation are derived from the ones imposed by the PlioMIP experiment 2, and atmospheric CO_2 concentration is fixed to 405 ppm [*Haywood et al*., 2011]. The ability of this particular state-of-the-art climate model to simulate the late Pliocene climate is assessed in *Haywood et al*. [2013a], and although the global SST warming simulated by the IPSL-CM5A model is in the lower range, it is comparable to other GCMs of the PlioMIP, such as CCSM4 and MRI-CGCM 2.3 models. It was recently shown that different insolation forcings provide important changes in simulated SSTs, especially on the annual cycle of SST [*Haywood et al*., 2013b]. To better capture the full range of climate variability that characterized the Late Pliocene, we also use different orbital parameters than those applied in the PlioMIP project which assigns modern orbital configuration. We apply two extreme orbital configurations which correspond to the maximum (Plio_max) and the minimum (Plio_min) summer solstice insolation occurring during the Late Pliocene at 65°N, based on *Laskar et al*. [2004] to force the IPSL-coupled model [*Contoux et al*., 2013].

5. Results and Discussion

[20] Temperature values estimated by *G. bulloides* Mg/Ca are colder than the alkenone-based SST estimation by ∼3 to 10°C over the studied time interval (Figure 5). Overall, the Mg/Ca-derived temperature estimations based on the leaching procedure leads to temperature estimates that marginally agree with the laser ablation-based temperature estimation (Figure 5), suggesting that the difference in SST estimates based on alkenones and Mg/Ca does not depend on the analytical technique used to measure foraminiferal Mg/Ca. Unlike in the alkenone-based SSTs, we do not detect any significant cooling trend in *G. bulloides* Mg/Ca associated with the increase in opal accumulation rate (Figure 5).

[21] Several processes other than temperature can affect the Mg/Ca-derived temperature estimates and might contribute to the SST contrast between the two paleothermometers. Dissolution is known to lower Mg/Ca because it preferentially removes Mg relative to Ca [see e.g., *Regenberg et al*., 2006]. Good preservation of foraminiferal tests illustrated in SEM indicated that dissolution is unlikely to have affected our coring site over the studied time interval (Figure 3). It is not surprising given that the dissolution proxies based on *G. bulloides* test preservation indicate no effect of dissolution down to a water depth of ∼3000 m and a lysocline deeper than 4000 m in the Cape Basin, South of the Walvis Ridge [*Henrich et al*., 2003]. Biologically mediated dissolution is somehow responsible for supra-lysoclinal dissolution in the Cape Basin, but takes place at water depths much greater than at the drilling site [*Henrich et al*., 2003].

[22] Salinity has also been shown to affect Mg/Ca in high-salinity environments such as the Red Sea [*Hoogakker et al*., 2009] and the Mediterranean Sea [*Ferguson et al*., 2008], and to a lesser extent in open ocean areas where surface salinities are above 35.5 [*Arbuszewski et al*., 2010; *Mathien-Blard and Bassinot*, 2009]. At coring site, however, neither surface nor subsurface waters reach salinities values of 35.5 [*Locarnini et al*., 2006]. We also note that a recent re-evaluation of the salinity effect on foraminiferal Mg/Ca points to a much lower Mg/Ca sensitivity to salinity changes than previously reported [*Hertzberg and Schmidt*, 2013; *Hönisch et al*., 2013].

[23] Finally, seawater Mg/Ca is thought to have changed over million-year time scales, and adjusting the Mg/Ca for long-term changes in seawater Mg/Ca has led to revising Pliocene-age equatorial Pacific SST toward warmer conditions by up to 2°C [*Medina-Elizalde et al*., 2008]. In *Medina-Elizalde et al*. [2008], the seawater Mg/Ca used in such correction was derived from indirect estimation of seawater Mg measurements performed on pore fluids revealing a rapid rise in seawater Mg/Ca over the last 10 Ma, with seawater Mg/Ca values of about 30% lower than modern values during the late Pliocene [*Fantle and DePaolo*, 2006]. As emphasized by *Broecker and Yu* [2011], such an increase over the last ∼3 Ma would be extreme as the residence time for seawater Mg is ∼13 Myr. We also note that a more recent study based on calcite carbonate veins indicates that the strong increase in seawater Mg/Ca that started at ∼30 Ma reached present-day values a few million years ago, suggesting essentially stable seawater Mg/Ca values over the last 10 Ma [*Rausch et al*., 2013]. Another difficulty is embedded in uncertainties in the relationship between the Mg partition coefficient in calcite and the seawater Mg/Ca [*Evans and Müller*, 2012]. Applying a 20%

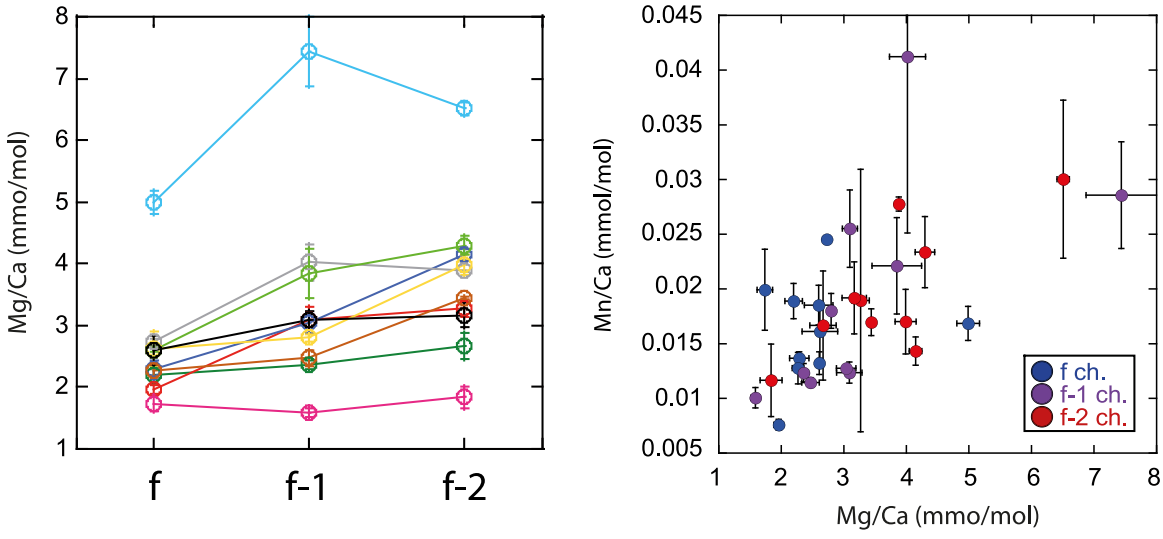

Figure 6. Example of one Late Pliocene sample dated at 2.9 Ma showing the Mg/Ca increase from the final to the f-2 chamber ((left) error bars indicate intrachamber standard deviation) and the relationship between Mg/Ca and Mn/Ca for the same sample ((right) error bars indicate intrachamber standard deviation).

reduction in seawater Mg/Ca and using the nonlinear correction between seawater Mg/Ca and foraminiferal Mg/Ca determined from inorganic calcite as done in *Medina-Elizalde et al.* [2008] would lead to adjusting the estimated temperatures toward temperatures warmer by a degree Celsius (see supporting information Figure S1[1]).

[24] We believe that none of the above-mentioned uncertainties can explain the alkenone-Mg/Ca contrast in estimated temperature, and now interpret Mg/Ca as estimates of ambient temperature when *G. bulloides* calcified its test. Reproducible modes of intrachamber, interchamber, and interspecimen Mg/Ca can be distinguished (Figure 6 and Table 1). As expected, the intrachamber variance is much lower than the interchamber and interspecimen variability over the entire data set (Figure 6 and Table 1). This indicates that the information contained in interchamber and interspecimen Mg/Ca can be used as indicators of the upper ocean temperature structure beyond analytical uncertainty. Overall, the coldest temperatures are consistently estimated from the final (*f*) chamber while the warmest temperatures are always estimated from the antepenultimate (*f-2*) chamber, with the penultimate (*f-1*) chamber accordingly providing intermediate temperature estimates (Figures 5 and 6). This pattern is in agreement with analogous Mg/Ca measurements performed on core tops from a Southwestern Pacific Ocean transect [*Marr et al.*, 2011], and highlights the potential of LA-ICPMS technique to capture different water depths as one would expect from the *G. bulloides* ontogeny because the species calcifies its last chambers within the thermocline [see e.g., *Schiebel and Hemleben*, 2005].

[25] Such inference is further supported by the observed relationship between Mg/Ca and Mn/Ca (Figure 6). Seawater Mn rapidly drops with water depth because Mn desorbing from aeolian material deposited at the sea surface by winds are rapidly adsorbed by particles and scavenged [*Statham et al.*, 1998]. Foraminiferal Mn/Ca have also been shown to reflect seawater Mn concentration as long as analytical techniques such as LA-ICP-MS or flow-through leaching procedures ensures that calcite Mn/Ca values are unambiguously unrelated to Mn-rich contaminant phases [*Klinkhammer et al.*, 2004]. Measurements of Mn/Ca performed on multiple planktonic foraminifera species occupying different water depth levels were then proposed to monitor past changes in the seawater Mn content induced by environmental parameters [*Klinkhammer et al.*, 2009]. One might expect the interchamber *G. bulloides* Mn/Ca contrast to portrait the vertical decrease recorded in seawater Mn occurring below the sea surface in the southeastern Atlantic [*Statham et al.*, 1998], if different water depth sampling were to be the explanation for the different Mg/Ca values measured on different chambers. We just find such a positive relationship between Mg/Ca and Mn/Ca (Figure 6), giving additional evidence that the

[1]Additional supporting information may be found in the online version of this article.

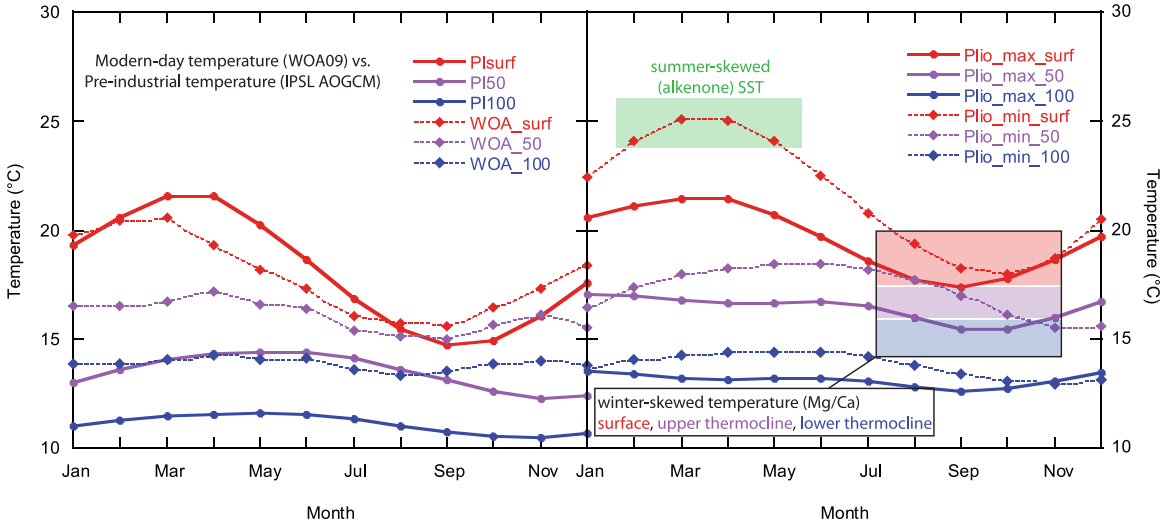

Figure 7. (left) Comparison between modern-day annual cycle of ocean temperature at studied site for surface, 50 and 100 m water depths as extracted from *Locarnini et al*. [2006] (dashed lines) and simulated by the IPSL-CM5A model [*Contoux et al*., 2012, 2013] (solid lines). (right) Late Pliocene annual cycle of ocean temperature at studied site for surface, 50 and 100 m water depths as simulated by the IPSL-CM5A model for the Plio_max (solid lines) and Plio_min (dashed lines) experiments [*Contoux et al*., 2012, 2013]. Rectangular boxes infer temperature range estimated between 3.3 and 3 Ma by alkenones (green rectangle) and Mg/Ca measured on f-2, f-1 and final chambers (red, purple and blue rectangles, respectively) as a function of hypothesized season likely to be captured by coccolithophorids and *G. bulloides* according to our conceptual model (see text for details).

interchamber temperature contrast can be attributed to different water depths.

[26] The proxy-dependent temperature offset might be explained by assuming that the two SST proxies are either strongly skewed toward warm (nonupwelling) and cold (upwelling) seasons for alkenones and Mg/Ca SST, respectively, and/or by the possibility that *G. bulloides* captures a temperature signal integrating a larger depth range in the water column as the relationship between Mg/Ca and Mn/Ca suggests (Figure 6). It is instructive to consider regional alkenone and Mg/Ca-based SST estimates to better encompass the full spectrum of SST captured by those two thermometers. Core-top values of alkenone-derived SST from the Angola Margin are ~20°C [*Kim et al*., 2002], while core-top values of Mg/Ca-derived temperatures performed on *G. bulloides* from the Namibian margin rather point to recent SST of ~13°C [*Farmer et al*., 2005]. This 7°C difference is two times larger than the mean-annual SST difference between the two sites that are situated at different latitudes [*Farmer et al*., 2005], indicating that both thermometers cannot be assigned to mean-annual temperature. Alkenone-derived SSTs estimated for core-top and late Pleistocene interglacial periods are close to 20°C, which agrees perfectly with modern summer SST (Figure 2). We do not have core-top Mg/Ca values at coring site, but late Pleistocene *G. bulloides* Mg/Ca derived from sites situated North [*Hessler et al*., 2011] and South [*Farmer et al*., 2005] of ODP site 1082 suggest that assigning *G. bulloides* to winter surface to subsurface temperature (i.e., ~16 and 14°C at our coring site, respectively, Figure 1) is realistic (Figures 1, 2, and 7). This is in line with sediment trap time series from a nearby site, that recorded two pulses of *G. bulloides* shell fluxes when the upwelling was active, but almost no shell flux when the upwelling was quiescent [*Giraudeau et al*., 2000].

[27] These lines of evidence suggest that the SST contrast recorded between alkenones and *G. bulloides* Mg/Ca is most likely embedded in differences in the ecological niches occupied by coccolithophorids and *G. bulloides*. *G. bulloides* thrives during upwelling events, and is hence suitable to monitor surface and subsurface temperature over time periods when upwelling intensifies. If we assume that coccolithophorids were mainly sampling the warm and stratified surface ocean during periods of the year when upwelling ceases, we can comment on the annual cycle of late Pliocene SST. Our study indicates that surface

temperatures during upwelling events likely captured by the f-2 chamber was colder by more than 5°C than alkenone-based SST prior to 3 Ma, and were followed by a smooth reduction of the SST contrast mainly induced by a SST decrease recorded by alkenones (Figure 5). Overall, the proxy-proxy comparison suggests a late Pliocene SST seasonality equal or larger than that seen nowadays (Figures 1 and 5). If any, a decrease of SST seasonality over the time interval studied might be mediated by decreasing summer SST under constant winter temperatures (Figure 5), i.e., not directly reflecting the upwelling season.

[28] A coherent pattern of decreasing temperature is captured from the f-2 to the final chamber, suggesting a temperature contrast between depths at which *G. bulloides* calcified those two chambers being ~3–5°C (Figure 5). This contrast would imply an equal or greater temperature difference between the surface and the subthermocline during winter when compared to nowadays assuming that *G. bulloides* dwells within the upper 200 m (Figure 1). For two samples, the SST estimated from all chambers were virtually the same, and were associated with anomalously low temperature captured by the f-2 chamber rather than an anomalously high temperature captured by the final chamber, leading to a SST contrast between alkenones and Mg/Ca of ~10°C. The mean temperature captured by the final chamber is estimated to be about 15°C over the entire time interval studied (Figure 5), which is close to modern-day temperature found at a depth of 50 m according to the World Ocean Atlas (WOA) [*Locarnini et al*., 2006] (Figure 1).

[29] We build a conceptual model that assigns SST proxies to different seasons and water depths. Namely, alkenone-derived SST might be skewed toward summer while Mg/Ca measurements performed on different *G. bulloides* chambers might capture different levels of the upper water column during upwelling events—i.e., during winter. Model simulations designed to reproduce the late Pliocene climate can provide a diagnostic for our conceptual model. The IPSL-CM5A-coupled model standard simulation of the late Pliocene using modern orbital parameters has been shown to compare well with other AOGCMs in the framework of the PlioMIP project [*Haywood et al*., 2013a].

[30] As a proof of concept, we first analyze the preindustrial model run. The comparison of the annual cycle of SST as simulated by this model with SST derived from the WOA indicates that the model performs well, despite inherent difficulties to capture the dynamic of complex environments such as the BUS (Figure 7). The annual cycle of subsurface temperature suggests that the model underestimates temperature and/or that the WOA overestimates temperature by ~2–3°C (Figure 7). Virtually, none of the models does capture perfectly the oceanic temperature, while the gridding procedure applied to the WOA might suffer from a lack of in situ observations below surface. Mooring deployment time series from the northern Benguela region suggest in situ temperature at 50 and 100 m seasonally varying between 12 and 13°C, and 11.5 and 12.5°C, respectively [*Mohrholz et al*., 2008], i.e., inferring subsurface temperature colder than estimated by the ocean atlas and suggesting that the model realistically captures modern-day ocean temperature.

[31] We now turn to seasonal temperature simulated for two insolation configurations of the late Pliocene at surface, 50 and 100 m water depths (Plio_min, Plio_max in Figure 7) to highlight the likely changes in the degree of the upper water column stratification. We stress that it is impossible to assign firm calcification water depths to the different chambers analyzed on *G. bulloides* because of multiple uncertainties that are associated with its thriving water depth range. By design, our conceptual model cannot be used to comment on the model performance based on *G. bulloides* ecology, or to attribute a water depth range for *G. bulloides* life cycle on the basis of the model output. Rather, we test the ability of our conceptual model to explain proxy-proxy mismatch in the light of the expected ecological niches occupied by coccolithophorids and *G. bulloides*.

[32] The IPSL-CM5A model output indicates that the alkenone-derived temperatures are in better agreement with the SSTs simulated for austral summer to early autumn between 3.3 and 3 Ma. In particular, alkenone temperatures match remarkably well to summer temperatures when the model is set up with the higher austral summer insolation (Plio_min experiment), while the Plio_max experiment simulates temperatures slightly colder than alkenones SST. The alkenone SST variability is, however, ~3°C between 3.3 and 3 Ma, which is comparable to the summer SST difference simulated between the Plio_min and the Plio_max experiments. The sampling resolution cannot resolve all the orbital configurations over the time interval studied, as it is lower than the precession index depicted at the top of Figure 5. Conversely,

Mg/Ca-derived temperatures better match with surface and subsurface temperature simulated for the austral winter to early spring (Figure 7). Highest fluxes of *G. bulloides* shown as gray bars on Figure 5 coincide, in general, to lowest fluxes of alkenones. The timing of high fluxes of alkenones and *G. bulloides* suggests that other processes operating on time scales longer than one precessional cycle probably affect the SST records. All together, those features suggest that our conceptual model that accounts for differences in ecological seasonality of planktonic organisms is valid (Figure 7). Accordingly, we assign both SST proxies to distinct ecological niches within the Late Pliocene time window over which orbital parameters possibly played some additional role in determining temperature at coring site.

[33] Although *G. bulloides* Mg/Ca has long been recognized as being associated with temperature conditions during upwelling seasons at low latitudes [see e.g., *Gupta et al*., 2003], the alkenone-based SSTs that best fit to mean-annual SSTs in the modern ocean are often assigned to mean-annual SST when applied to past geological times [*Müller et al*., 1998]. From an evolutionary perspective, diatoms have evolved a nutrient storage vacuole and thrive best in regions where high nutrient supply to the sea surface occurs sporadically, such as coastal upwelling, eventually outcompeting coccolithophorids that thrive over seasons when surface waters stratify [*Falkowski et al*., 2004]. This led diatoms and coccolithophorids opting for an ecological divergence, with diatoms following opportunistic strategies while coccolithophorids grow under more stratified water conditions [*Iglesias-Rodriguez et al*., 2002; *Falkowski et al*., 2004]. Nowadays, phytoplankton community distribution in the Atlantic Ocean reflects this ecological divergence, where the relative distribution of diatoms and coccolithophorids is used to track nutrient supply to the upper mixed layer [*Cermeño et al*., 2008]. Consequently, coccolithophorids and, by inference, alkenone-based proxies such as SST and primary productivity might not be accurate recorders of upwelling intensity per se.

[34] Our suggestion that alkenone-based SSTs in the BUS might represent warm season SSTs has, if applicable to other upwelling systems, implications for Pliocene evolution of upwelling systems. On the one hand, *G. bulloides* Mg/Ca-based estimates of surface and subsurface temperatures at times of intensified upwelling were probably not warmer by more than ~2°C during the Pliocene than today, evolving at the surface from ~18 to ~16°C, and probably at the base of the thermocline from ~15 to ~14°C (Figures 1 and 5). On the other hand, alkenone-based SST suggest a cooling by up to 6°C over the last 3.5 Ma, evolving from ~26 to ~20°C. It suggests that the BUS seasonality decreased over the last 3.5 Ma. Today, the modern annual cycle in SST and in primary productivity is less marked in the BUS than in other upwelling systems [*Chavez and Messié*, 2009]. Further multiproxy SST studies must be conducted in other upwelling systems to assess whether the peculiarity of the BUS seasonality with respect to other upwelling systems can be attributed to asymmetric changes in winter and summer SST.

[35] Hence, on basis of the data we have in hands, we find it difficult to use alkenone-based SSTs and alkenone MAR as reliable indicators for the upwelling season because alkenones seem to capture hydrological features over times when upwelling ceases (Figure 5). Rather, alkenone-based SST jointly used with Mg/Ca temperature records based on upwelling-skewed planktonic foraminifera might provide more accurate estimates of the status of past upwelling intensity and seasonality because *G. bulloides* likely captures surface and subsurface temperature reflective of the upwelling season (Figure 5). We are also cautious in interpreting *G. bulloides* Mg/Ca as an evidence that intensified upwelling prevailed over the late Pliocene. While warm and cold temperature values occurring during seasonal extremes may not have changed much over this time window, *G. bulloides* fluxes were occurring unevenly between 3.5 and 2 Ma (Figure 5), indicating that cold temperatures captured by *G. bulloides* might occur as pulses when favorable conditions for upwelling prevailed. Rather, changes in the upwelling seasonal time window during which upwelling intensifies or ceases may explain the opal MAR increase observed over the studied time interval, probably acting synergistically with changes in the pathways by which silicate was supplied to the euphotic zone [*Etourneau et al*., 2012].

[36] For subtropical coastal upwelling, SSTs during the Pliocene are exclusively derived from alkenones and subsequently used as templates for Pliocene SSTs in upwelling zones [*Fedorov et al*., 2013]. Extreme alkenone-derived SST decreases, however, might not be reflective of intensification of upwelling and/or of a cooling of subsurface water fuelling the upper mixed layer, but rather of a cooling predominantly affecting the warm and

stratified season. Our finding that *G. bulloides* Mg/Ca provides winter surface and subsurface temperature estimates only slightly warmer than at present-day should be considered while attempting to identify physical mechanisms related to subtropical mixing [*Fedorov et al*., 2010, 2013], since it appears that the seasonal thermocline in the BUS and other subtropical upwelling systems were probably undersampled in previous studies based only on alkenones [*Dekens et al*., 2007]. Whether some aspects of seasonality and subsurface temperatures that we have observed in the BUS may apply elsewhere during the late Pliocene clearly needs to be investigated by performing multiproxy SST estimations. Recent work by *Friedrich et al*. [2013] comparing alkenone and Mg/Ca-derived SST for clarifying some aspects of the North Atlantic current variability during the late Pliocene seems to go into the same direction.

6. Conclusion

[37] We reassessed SST estimates of past upwelling temperature conditions in the upper water column in the Benguela region during the late Pliocene. We compared SST proxies likely to be reflective of either different seasons and/or different water depths and built a scenario that accounts for ecological niches occupied by the different planktonic organisms when constraining temperature variability. Our conceptual model agrees well with seasonal temperatures as simulated in the upper water column by a state-of-the-art coupled climate model (IPSL-CM5A), and implies only moderately warmer temperatures during the late Pliocene when seasonality and upper water column stratification are considered. We believe that if the specific features of the different temperature proxies are taken into account in future studies, this will help to unravel some aspects of the late Pliocene climate warmth conundrums that were previously pointed out in model/data comparison exercises, and refine our understanding of key parameters involved in picturing how upwelling systems likely behaved during that period.

Acknowledgments

[38] We thank Graham Mortyn for fruitful discussion and Martin Medina-Elizalde for his help with calculating the Mg/Ca with respect to secular changes in seawater Mg concentrations. We also warmly thank one anonymous reviewer and David Evans for insightful comments that improved the manuscript.

References

Arbuszewski, J., P. deMenocal, A. Kaplan, and E. C. Farmer (2010), On the fidelity of shell-derived $\delta^{18}O_{seawater}$ estimates, *Earth Planet. Sci. Lett.*, *300*, 185–196.

Barker, S., I. Cacho, H. Benway, and K. Tachikawa (2005), Planktonic foraminiferal Mg/Ca as a proxy for past oceanic temperatures: A methodological overview and data compilation for the Last Glacial Maximum, *Quat. Sci. Rev.*, *24*, 821–834.

Bassinot, F. C., C. Marzin, P. Braconnot, O. Marti, E. Mathien-Blard, F. Lombard, and L. Bopp (2011), Holocene evolution of summer winds and marine productivity in the tropical Indian Ocean in response to insolation forcing: Data-model comparison, *Clim. Past*, *7*, 815–829.

Berger, W. H., C. B. Lange, and M. E. Pérez (2002), The early Matuyama Diatom Maximum off SW Africa: A conceptual model, *Mar. Geol.*, *180*, 105–116.

Birch, H., H. K. Coxall, P. N. Pearson, D. Kroon, and M. O'Regan (2013), Planktonic foraminifera stable isotopes and water column structure: Disentangling ecological signals, *Mar. Micropaleontol.*, *101*, 127–145.

Braconnot, P., S. P. Harrison, M. Kageyama, P. J. Bartlein, V. Masson-Delmotte, A. Abe-Ouchi, B. Otto-Bliesner, and Y. Zhao (2012), Evaluation of climate models using palaeoclimatic data, *Nat. Clim. Change*, *2*, 417–424, doi:10.1038/nclimate1456.

Broecker, W., and J. Yu (2011), What do we know about the evolution of Mg to Ca ratios in seawater? *Paleoceanography*, *26*, PA3203, doi:10.1029/2011PA002120.

Cermeño, P., S. Dutkiewicz, R. P. Harris, M. Follows, O. Schofield, and P. G. Falkowski (2008), The role of nutricline depth in regulating the ocean carbon cycle, *Proc. Natl. Acad. Sci. U. S. A.*, *105*, 20,344-20,349.

Chavez, F. P., and M. Messié (2009), A comparison of Eastern Boundary Upwelling Ecosystems, *Prog. Oceanogr.*, *83*, 80–96.

Cléroux, C., E. Cortijo, P. Anand, L. Labeyrie, F. Bassinot, N. Caillon, and J.-C. Duplessy (2008), Mg/Ca and Sr/Ca ratios in planktonic foraminifera: Proxies for upper water column temperature reconstruction, *Paleoceanography*, *23*, PA3214, doi:10.1029/2007PA001505.

Contoux, C., G. Ramstein, and A. Jost (2012), Modelling the mid-Pliocene Warm Period climate with the IPSL coupled model and its atmospheric component LMDZ5A, *Geosci. Model Dev.*, *5*, 903–917, doi:10.5194/gmd-5-903-2012.

Contoux, C., A. Jost, G. Ramstein, P. Sepulchre, G. Krinner, and M. Schuster (2013), Megalake Chad impact on climate and vegetation during the late PLiocene and the mid-Holocene. *Clim. Past*, *9*, 1417–1430.

de Villiers, S., M. Graves, and H. Elderfield (2002), An intensity ratio calibration method for the accurate determination of Mg/Ca and Sr/Ca of marine carbonates by ICP-AES, *Geochem. Geophys. Geosyst.*, *3*(1), 1001, doi:10.1029/2001GC000169.

Dekens, P. S., D. W. Lea, D. K. Pak, and H. J. Spero (2002), Core top calibration of Mg/Ca in the tropical foraminifera: Refining paleotemperature estimation, *Geochem. Geophys. Geosyst.*, *3*(4), 1022, doi:10.1029/2001GC000200.

Dekens, P. S., A. C. Ravelo, and M. D. McCarthy (2007), Warm upwelling regions in the Pliocene warm period, *Paleoceanography*, *22*, PA3211, doi:10.1029/2006PA001394.

Dittert, N., and R. Henrich (2000), Carbonate dissolution in the South Atlantic Ocean: Evidence from ultrastructure breakdown in *Globigerina bulloides*, *Deep Sea Res., Part I*, *47*, 603–620.

Dowsett, H. J., M. M. Robinson, and K. M. Foley (2009), Pliocene three-dimensional global ocean temperature reconstruction, *Clim. Past*, *5*, 769–783, doi:10.5194/cp-5-769-2009.

Dowsett, H. J., et al. (2012), An assessment of confidence in Pliocene global sea-surface temperature, *Nat. Clim. Change*, *2*, 365–371, doi:10.1038/nclimate1455.

Elderfield, H., and G. Ganssen (2000), Past temperature and $\delta^{18}O$ of surface ocean waters inferred from foraminiferal Mg/Ca ratios, *Nature*, *405*, 442–445.

Erez, J. (2003), The source of ions for biomineralization in foraminifera and their implications for paleoceanographic proxies, *Rev. Mineral. Geochem.*, *54*, 115–149.

Etourneau, J., P. Martinez, T. Blanz, and R. Schneider (2009), Pliocene-Pleistocene variability of upwelling activity, productivity, and nutrient cycling in the Benguela region, *Geology*, *37*, 871–874.

Etourneau, J., C. Ehlert, M. Frank, P. Martinez, and R. Schneider (2012), Contribution of changes in opal productivity and nutrient distribution in the coastal upwelling systems to Late Pliocene/Early Pleistocene climate cooling, *Clim. Past*, *8*, 1435–1445.

Evans, D., and W. Müller (2012), Deep time foraminifera Mg/Ca paleothermometry: Nonlinear correction for secular change in seawater Mg/Ca, *Paleoceanography*, *27*, PA4205, doi:10.1029/2012PA002315.

Falkowski, P. G., M. E. Katz, A. H. Knoll, A. Quigg, J. A. Raven, O. Schofield, and F. J. R. Taylor (2004), The evolution of modern eukaryotic phytoplankton, *Science*, *305*, 354–360.

Fantle, M. S., and D. J. DePaolo (2006), Sr isotopes and pore fluid chemistry in carbonate sediment of the Ontong Java Plateau: Calcite recrystallization rates and evidence for a rapid rise in seawater Mg over the last 10 million years, *Geochim. Cosmochim. Acta*, *70*, 3883–3904.

Farmer, E. C., P. deMenocal, and T. Marchitto (2005), Holocene and deglacial ocean temperature variability in the Benguela upwelling region: Implications for low-latitude atmospheric circulation, *Paleoceanography*, *20*, PA2018, doi:10.1029/2004PA001049.

Fedorov, A. V., C. Brierley, and K. Emanuel (2010), Tropical cyclones and permanent El Nino in the early Pliocene epoch, *Nature*, *463*, 1066–1070.

Fedorov, A. V., K. Lawrence, Z. Liu, C. Brierley, P. Dekens, and A. C. Ravelo (2013), Patterns and Mechanisms of early Pliocene warmth, *Nature*, *496*, 43–49.

Ferguson, J. E., G. M. Henderson, M. Kucera, and R. E. M. Rickaby (2008), Systematic change of foraminiferal Mg/Ca ratios across a strong salinity gradient, *Earth Planet. Sci. Lett.*, *265*, 153–166.

Fricker, M. B., D. Kutscher, B. Aeschlimann, J. Frommer, R. Dietiker, J. Bettmer, and D. Günther (2011), High spatial resolution trace element analysis by LA-ICP-MS using a novel ablation cell for multiple or large samples, *Int. J. Mass Spectrom.*, *307*, 39–45.

Friedrich, O., R. Schiebel, P. A. Wilson, S. Weldeab, C. J. Beer, M. J. Cooper, and J. Fiebig (2012), Influence of test size, water depth, and ecology on Mg/Ca, Sr/Ca, $\delta^{18}O$ and $\delta^{13}C$ in nine modern species of planktic foraminifers, *Earth Planet. Sci. Lett.*, *319–320*, 133–145.

Friedrich, O., P. A. Wilson, C. T. Bolton, C. J. Beer, and R. Schiebel (2013), Late Pliocene to early Pleistocene changes in the North Atlantic Current and suborbital-scale sea-surface temperature variability, *Paleoceanography*, *28*, 274–282, doi:10.1002/palo.20029.

Giraudeau, J. (1993), Planktonic foraminiferal assemblages in surface sediments from the southwest African continental margin, *Mar. Geol.*, *110*, 47–62.

Giraudeau, J., G. W. Bailey, and C. Pujol (2000), A high-resolution time-series analyses of particle fluxes in the Northern Benguela coastal upwelling system: Carbonate record of changes in biogenic production and particle transfer processes, *Deep Sea Res., Part II*, *27*, 1999–2028.

Greaves, M., et al. (2008), Interlaboratory comparison study of calibration standards for foraminiferal Mg/Ca thermometry, *Geochem. Geophys. Geosyst.*, *9*, Q08010, doi:10.1029/2008GC001974.

Gupta, A. K., D. M. Anderson, and J. T. Overpeck (2003), Abrupt changes in the Asian southwest monsoon during the Holocene and their links to the North Atlantic Ocean, *Nature*, *421*, 354–357.

Haywood, A. M., H. J. Dowsett, M. M. Robinson, D. K. Stoll, A. M. Dolan, D. J. Lunt, B. Otto-Bliesner, and M. A. Chandler (2011), Pliocene Model Intercomparison Project (PlioMIP): Experimental design and boundary conditions (Experiment 2), *Geosci. Model Dev.*, *4*, 571–577.

Haywood, A. M., et al. (2013a), Large-scale features of Pliocene climate: Results from the Pliocene Model Intercomparison Project, *Clim. Past*, *9*, 191–209.

Haywood, A. M., et al. (2013b), On the identification of a Pliocene time slice for data-model comparison, *Philos. Trans. R. Soc. A*, *371*, 20120515.

Henrich, R., K.-H. Baumann, S. Gerhardt, M. Gröger, and A. N. A. Volbers (2003), Carbonate preservation in deep and intermediate water masses in the South Atlantic: Evaluation and geological record (a review), in *The South Atlantic in the Late Quaternary: Reconstructions of Material Budgets and Current Systems*, edited by G. Wefer, S. Mulitza, and V. Ratmeyerl, pp. 645–670, Springer, Berlin.

Hertzberg, J. E., and M. W. S. Schmidt (2013), Refining Globigerinoides ruber Mg/Ca paleothermometry in the Atlantic Ocean, *Earth Planet. Sci. Lett.*, *383*, 123–133.

Hessler, I., S. Steinke, J. Groeneveld, L. Dupont, and G. Wefer (2011), Impact of abrupt climate change in the tropical southeast Atlantic during Marine Isotope Stage (MIS) 3, *Paleoceanography*, *26*, PA4209, doi:10.1029/2011PA002118.

Hönisch, B., K. Allen, D. W. Lea, H. J. Spero, S. Eggins, J. Arbuszewski, P. deMenocal, Y. Rosenthal, A. D. Russell, and H. Elderfield (2013), The influence of salinity on Mg/Ca in planktic foraminifers—Evidence from cultures, core-top sediments and complementary $\delta^{18}O$, *Geochim. Cosmochim. Acta*, *121*, 196–213.

Hoogakker, B. A. A., G. P. Klinkhammer, H. Elderfield, E. J. Rohling, and C. Hayward (2009), Mg/Ca paleothermometry in high salinity environments, *Earth Planet. Sci. Lett.*, *284*, 583–589.

Iglesias-Rodriguez, M. D., C. W. Brown, S. C. Doney, J. Kleypas, D. Kolber, Z. Kolber, P. K. Hayes, and P. G. Falkowski (2002), Representing key phytoplankton functional groups in ocean carbon cycle models: Coccolithophorids, *Global Biogeochem. Cycles*, *16*(4), 1100, doi:10.1029/2001GB001454.

Jochum, K. P., U. Weis, B. Stoll, D. Kuzmin, Q. Yang, I. Raczek, D. E. Jacob, A. Stracke, K. Birbaum, D. A. Frick, D. Günther, and J. Enzweiler (2011), Determination of reference values for NIST SRM 610–617 glasses following ISO guidelines. *Geostandards Geoanalytical Res.*, *35*, 397–429. doi: 10.1111/j.1751-908X.2011.00120.x.

Kim, J. H., R. R. Schneider, P. J. Muller, and G. Wefer (2002), Interhemispheric comparison of deglacial sea-surface temperature patterns in Atlantic eastern boundary currents, *Earth Planet. Sci. Lett.*, *194*, 383–393.

Klinkhammer, G. P., B. A. Haley, A. C. Mix, H. M. Benway, and M. Cheseby (2004), Evaluation of automated flow-through time-resolved analysis of foraminifera for Mg/Ca paleothermometry, *Paleoceanography*, *19*, PA4030, doi: 10.1029/2004PA001050.

Klinkhammer, G. P., A. C. Mix, and B. A. Haley (2009), Increased dissolved terrestrial input to the coastal ocean during the last deglaciation, *Geochem. Geophys. Geosyst.*, *10*, Q03009, doi:10.1029/2008GC002219.

Lange, C. B., W. H. Berger, H.-L. Lin, G. Wefer, and Shipboard Scientific Party leg 175 (1999), The early Matuyama Diatom maximum off SW Africa, Benguela current system (ODP leg 175), *Mar. Geol.*, *161*, 93–114.

Laskar, J. (1990), The chaotic motion of the solar system: A numerical estimate of the size of the chaotic zones, *Icarus*, *88*, 266–291.

Laskar, J., P. Robutel, F. Joutel, M. Gastineau, A. C. M. Correia, and B. Levrard (2004), A long term numerical solution for the insolation quantities of the Earth, *Astron. Astrophys.*, *428*, 261–285.

Lea, D. W., T. A. Mashiotta, and H. J. Spero (1999), Controls on magnesium and strontium uptake in planktonic foraminifera determined by live culturing, *Geochim. Cosmochim. Acta*, *63*, 2369–2379.

Leduc, G., R. R. Schneider, J.-H. Kim, and G. Lohmann (2010a), Holocene and Eemian sea surface temperature trends as revealed by alkenone and Mg/Ca paleothermometry, *Quat. Sci. Rev.*, *29*, 989–1004.

Leduc, G., C. T. Herbert, T. Blanz, P. Martinez, and R. Schneider (2010b), Contrasting evolution of sea surface temperature in the Benguela upwelling system under natural and anthropogenic climate forcings, *Geophys. Res. Lett.*, *37*, L20705, doi:10.1029/2010GL044353.

Lisiecki, L. E., and M. E. Raymo (2005), A Pliocene-Pleistocene stack of 57 globally distributed benthic d18O records, *Paleoceanography*, *20*, PA1003, doi:10.1029/2004PA001071.

Locarnini, R. A., A. V. Mishonov, J. I. Antonov, T. P. Boyer, and H. E. Garcia (2006), World Ocean Atlas 2005, vol. *1*, in Temperature, edited by S. Levitus, 182 pp., NOAA Atlas NESDIS 61, U.S. Gov. Print. Off., Washington, D. C.

Lohmann, G., M. Pfeiffer, T. Laepple, G. Leduc, and J.-H. Kim (2013), A model-data comparison of the Holocene global sea surface temperature evolution, *Clim. Past.*, *9*, 1807–1839, doi:10.5194/cp-9-1807-2013.

Lombard, F., L. Labeyrie, E. Michel, L. Bopp, E. Cortijo, S. Retailleau, H. Howa, and F. Jorissen (2011), Modelling planktic foraminifer growth and distribution using an eco-physiological multispecies approach, *Biogeosciences*, *8*, 853–873, doi:10.5194/bg-8-853-2011.

Medina-Elizalde, M., D. W. Lea, and M. S. Fantle (2008), Implications of seawater Mg/Ca variability for Plio-Pleistocene tropical climate reconstruction, *Earth Planet. Sci. Lett.*, *269*, 584–594.

Marr, J. P., J. A. Baker, L. Carter, A. S. R. Allan, G. B. Dunbar, and H. C. Bostock (2011), Ecological and temperature controls on Mg/Ca ratios of *Globigerina bulloides* from the southwest Pacific Ocean, *Paleoceanography*, *26*, PA2209, doi:10.1029/2010PA002059.

Martin, P. A., and D. W. Lea (2002), A simple evaluation of cleaning procedures on fossil benthic foraminiferal Mg/Ca, *Geochem. Geophys. Geosyst.*, *3*(10), 8401, doi:10.1029/2001GC000280.

Mathien-Blard, E., and F. Bassinot (2009), Salinity bias on the foraminifera Mg/Ca thermometry: Correction procedure and implications for past ocean hydrographic reconstructions, *Geochem. Geophys. Geosyst.*, *10*, Q12011, doi:10.1029/2008GC002353.

McConnell, M. C., and R. C. Thunell (2005), Calibration of the planctonic foraminiferal Mg/Ca paleothermometer: Sediment trap results from the Guaymas Basin, Gulf of California, *Paleoceanography*, *20*, PA2016, doi:10.1029/2004PA001077.

Mohrholz, V., C. H. Bartholomae, A. K. van der Plas, and H. U. Lass (2008), The seasonal variability of the northern Benguela undercurrent and its relation to the oxygen budget on the shelf, *Cont. Shelf Res.*, *28*, 424–441.

Moroshkin, K. V., V. A. Bubnov, and R. P. Bulatov (1970), Water circulation in the eastern South Atlantic Ocean, *Oceanology*, *10*, 27–34.

Mortyn, P. G., and C. D. Charles (2003), Planktonic foraminiferal depth habitat and $\delta^{18}O$ calibrations: Plankton tow results from the Atlantic sector of the Southern Ocean, *Paleoceanography*, *18*(2), 1037, doi:10.1029/2001PA000637.

Müller, P. J., G. Kirst, G. Ruhland, I. von Storch, and A. Rosell-Melé (1998), Calibration of the alkenone paleotemperature index Uk'37 based on core-tops from the eastern South Atlantic and the global ocean (60°N–60°S), *Geochim. Cosmochim. Acta*, *62*, 722–1757.

Narayan, N., A. Paul, S. Mulitza, and M. Schulz (2010), Trends in coastal upwelling intensity during the late 20th century, *Ocean Sci.*, *6*, 815–823.

Pena, L. D., E. Calvo, I. Cacho, S. Eggins, and C. Pelejero (2005), Identification and removal of Mn-Mg-rich contaminant phases on foraminiferal tests: Implications for Mg/Ca past temperature reconstructions, *Geochem. Geophys. Geosyst.*, *6*, Q09P02, doi:10.1029/2005GC000930.

Pena, L. D., I. Cacho, E. Calvo, C. Pelejero, S. Eggins, and A. Sadekov (2008), Characterization of contaminant phases in foraminifera carbonates by electron microprobe mapping, *Geochem. Geophys. Geosyst.*, *9*, Q07012, doi:10.1029/2008GC002018.

Rausch, S., F. Böhm, W. Bach, A. Klügel, and A. Eisenhauer (2013), Calcium carbonate veins in ocean crust record a threefold increase of seawater Mg/Ca in the past 30 Million years, *Earth Planet. Sci. Lett.*, *362*, 215–224.

Regenberg, M., D. Nürnberg, S. Steph, J. Groeneveld, D. Garbe-Schönberg, R. Tiedemann, and W.-C. Dullo (2006), Assessing the effect of dissolution on planktonic foraminiferal Mg/Ca ratios: Evidence from Caribbean core tops, *Geochem. Geophys. Geosyst.*, *7*, Q07P15, doi:10.1029/2005GC001019.

Rosell-Melé, A., and F. G. Prahl (2013), Seasonality of $U^{K'}_{37}$ temperature estimates as inferred from sediment trap data, *Quat. Sci. Rev.*, *72*, 128–136.

Rosell-Melé A., A. Martínez-Garcia, and E. L. McClymont (2014), Persistent warmth across the Benguela upwelling system during the Pliocene epoch, *Earth Planet. Sci. Lett. 386*, 10–20.

Rosell-Melé, A., et al. (2001), Precision of the current methods to measure the alkenone proxy $U^{K'}_{37}$ and absolute alkenone abundance in sediments: Results of an interlaboratory comparison study, *Geochem. Geophys. Geosyst.*, *2*(7), 1046, doi: 10.1029/2000GC000141.

Sadekov, A. Y., S. M. Eggins, and P. De Deckker (2005), Characterization of Mg/Ca distributions in planktonic foraminifera species by electron microprobe mapping, *Geochem. Geophys. Geosyst.*, *6*, Q12P06, doi:10.1029/2005GC000973.

Schiebel, R., and C. Hemleben (2005), Modern planktic foraminifera, *Paläontologische Z.*, *79*, 135–148.

Schneider, B., G. Leduc, and W. Park (2010), Disentangling seasonal signals in Holocene climate trends by satellite-model-proxy integration, *Paleoceanography*, *25*, PA4217, doi:10.1029/2009PA001893.

Shannon, L. V. (1985), The Benguela Ecosystem Part 1: Evolution of the Benguela, physical features and processes, *Oceanogr. Mar. Biol.*, *23*, 105–182.

Skinner, L. C., and H. Elderfield (2005), Constraining ecological and biological bias in planktonic foraminiferal Mg/Ca and $\delta^{18}O_{cc}$: A multispecies approach to proxy calibration testing, *Paleoceanography*, *20*, PA1015, doi:10.1029/2004PA001058.

Spero, H. J., and D. W. Lea (1996), Experimental determination of stable isotope variability in *Globigerina bulloides*: Implications for paleoceanographic reconstruction, *Mar. Micropaleontol.*, *28*, 231–246.

Statham, P. J., P. A. Yeats, and W. M. Landing (1998), Manganese in the eastern Atlantic Ocean: Processes influencing deep and surface water distributions, *Mar. Chem.*, *61*, 55–68.

Tachikawa, K., S. Sepulcre, T. Toyofuku, and E. Bard (2008), Assessing influence of diagenetic carbonate dissolution on planktonic foraminiferal Mg/Ca in the southeastern Arabian Sea over the past 450 ka: Comparison between *Globigerinoides ruber* and *Globigerinoides sacculifer*, *Geochem. Geophys. Geosyst.*, *9*, Q04037, doi:10.1029/2007GC001904.

Wang, Y. V., G. Leduc, M. Regenberg, N. Andersen, T. Larsen, T. Blanz, and R. R. Schneider (2013), Northern and southern hemisphere controls on seasonal sea surface temperatures in the Indian Ocean during the last deglaciation, *Paleoceanography*, *28*, doi:10.1002/palo.20053, in press.

Žarić, S., B. Donner, G. Fischer, S. Mulitza, and G. Wefer (2005), Sensitivity of planktic foraminifera to sea surface temperature and export production as derived from sediment trap data, *Mar. Micropaleontol.*, *55*, 75–105.